Effects of nuclear orientation on the mass distribution of fission fragments in the reaction of $^{36}S+^{238}U$

K. Nishio,[1] H. Ikezoe,[1] S. Mitsuoka,[1] I. Nishinaka,[1] Y. Nagame,[1] Y. Watanabe,[2] T. Ohtsuki,[3] K. Hirose,[3] and S. Hofmann[4,5]

[1]*Japan Atomic Energy Agency, Tokai, Ibaraki 319-1195, Japan*

[2]*Institute of Particle and Nuclear Studies, High Energy Accelerator Research Organization (KEK), Tsukuba, Ibaraki 305-0801, Japan*

[3]*Laboratory of Nuclear Science, Tohoku University, Sendai 982-0826, Japan*

[4]*Gesellschaft für Schwerionenforschung mbH, D-64291 Darmstadt, Germany*

[5]*Institut für Kernphysik, Johann Wolfgang Goethe-Universität, D-60486 Frankfurt am Main, Germany*

(Received 5 December 2007; published 18 June 2008)

Fragment mass distributions for fission after full momentum transfer were measured for the reaction $^{36}S+^{238}U$ at bombarding energies around the Coulomb barrier. The data revealed a transition from symmetry to asymmetry mass distributions when the beam energies were decreased from above-barrier to sub-barrier values. The main components of the asymmetric mass distribution are at $A_H \approx 200$ and $A_L \approx 74$. The asymmetric fission is attributed to quasifission of the reacting system at polar collisions, whereas the symmetric fission originates from the compound nucleus produced in equatorial collisions. The results suggest a strong influence of orientation effects of the deformed target nuclei on fusion.

DOI: 10.1103/PhysRevC.77.064607 PACS number(s): 25.70.Jj, 25.85.Ge, 25.60.Pj, 24.10.Eq

I. INTRODUCTION

Superheavy elements have been successfully produced using two types of fusion reactions which differ by the amount of excitation energy of the compound nuclei. Cold-fusion reactions based on lead or bismuth targets result in low [1,2], whereas hot-fusion reactions based on actinide targets result in high excitation energy. However, using ^{48}Ca beams also in this case the excitation energies are relatively low [3].

Another difference between the two reactions is associated with the static deformation of the target nuclei. Since nuclei of the actinides are prolately deformed, the Coulomb-barrier height depends on the orientation of the target nucleus, and reactions start from different touching configurations. The two extreme cases are collisions with the polar and equatorial sides of the target nucleus. At low projectile energy nuclear contact occurs only at polar collisions, whereas at higher energy contact is obtained also in equatorial collisions. Orientation effects on fusion were investigated in reactions using deformed nuclei of rare-earth elements [4]. It was observed that equatorial collisions result in fusion, whereas polar collisions do not lead to fusion. The measured evaporation residue cross sections for $^{48}Ca+^{238}U$ and $^{48}Ca+^{242,244}Pu$ [3,5] have maxima at a bombarding energy close to the barrier for equatorial collisions, suggesting a higher fusion probability at this orientation. Similarly, orientation effects on fusion were measured for the reaction $^{30}Si+^{238}U$ [6].

In reactions with the light projectile ^{16}O with a ^{238}U target, the system results in fusion even at deep sub-barrier energies. In this case fusion is independent from the orientation [7]. Measured fission-fragment mass distributions revealed symmetric shapes for all projectile energies from above-barrier to sub-barrier values [8]. These results show that a symmetric mass distribution is characteristic for the formation of a heavy excited compound nucleus.

In reactions using the heavier projectile ^{48}Ca and targets of ^{238}U and ^{244}Pu, the fragment-mass distributions were measured at bombarding energies corresponding to the Bass barrier [9] which is slightly lower than the barrier for equatorial collisions. In this case the fragment-mass distribution was dominated by an asymmetric distribution with a mass of the heavy fragment at around $A_H \approx 208$. This phenomenon was attributed to quasifission, and the result implies that fusion-fission and quasifission have different mass distributions. In a reaction where fusion is influenced by orientation effects, we expect an increase of asymmetric fission at sub-barrier energies due to an increase of quasifission at polar collisions. In the present work we have measured fragment-mass distributions for the reaction $^{36}S+^{238}U$ in order to study a transition from quasifission to compound-nucleus fission as function of the bombarding energy.

In our measurements we selected those fission events which occurred after the momentum of the projectile was fully transferred to the composite system. The full momentum transfer (FMT) fissions were separated from fission events following nucleon transfer, which also occurs when fissile targets like ^{238}U are used.

II. EXPERIMENT

Beams of 163–208 MeV ^{36}S were supplied by the JAEA-tandem accelerator. Beam intensities were in the range from 0.1 to 1.0 particle-nA. The ^{238}U target was prepared by electrodeposition of natural UO_2 on a Ni backing of 90 $\mu g/cm^2$ thickness with a diameter of 5 mm. The thickness of the ^{238}U contents was 82 $\mu g/cm^2$.

The target was mounted at an angle of 45° to the beam axis with the Ni backing oriented downstream. Two fission fragments (FFs) were detected in coincidence by position-

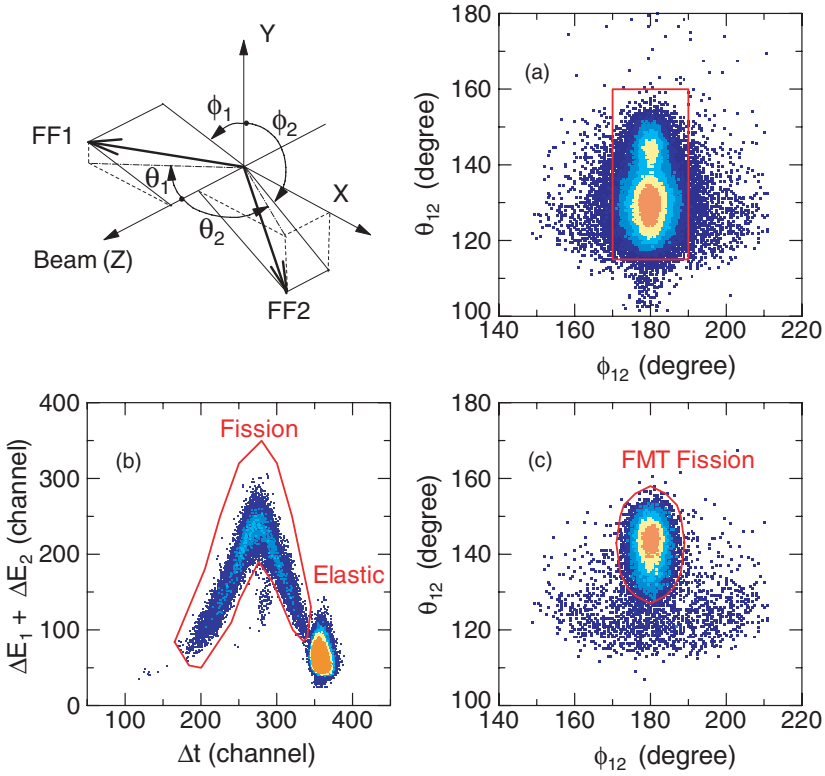

FIG. 1. (Color online) (Upper left) Definition of the emission angles θ_1 and θ_2 and of the out-of-plane angles ϕ_2 and ϕ_2. (a) Events plotted on the ϕ_{12} vs θ_{12} plane. (b) Plot on the Δt and $(\Delta E_1 + \Delta E_2)$ plane for events entering in the rectangular region in (a). (c) Same as (a), but obtained with a gate on the fission events as shown in (b).

sensitive multi-wire proportional counters (MWPCs). The emission angles θ_1 and θ_2 of FF1 and FF2 projected on the X-Z plane and the out-of-plane angles ϕ_1 and ϕ_2 were measured as defined in Fig. 1.

The MWPCs have an active area of 200 mm$\times$120 mm in horizontal and vertical direction, respectively. The detectors were operated with isobutane gas at a pressure of 3 Torr. A 3 μm Mylar film was used as an entrance window.

The detectors were located on both sides of the target each at a distance of 211 mm and at angles of $\theta_1 = -61.0^\circ$ for MWPC1 and $\theta_2 = +90.0^\circ$ for MWPC2. Each MWPC covers the emission angles of $-86.0^\circ \leqslant \theta_1 \leqslant -36.0^\circ$ and $65.0^\circ \leqslant \theta_2 \leqslant 115.0^\circ$. For the out-of-plane angle, the MWPC1 covers the range of $72.0^\circ \leqslant \phi_1 \leqslant 108.0^\circ$ at $\theta_1 = -61^\circ$, and the MWPC2 covers the range of $74.1^\circ \leqslant \phi_2 \leqslant 105.9^\circ$. We define the angles θ_{12} and ϕ_{12} between the two fragments as $\theta_2 - \theta_1$ and $\phi_1 + \phi_2$, respectively. Resolution to measure the $\theta_{1,2}$ is $0.9^\circ \sim 1.1^\circ$, and that for $\phi_{1,2}$ is $0.9^\circ \sim 1.5^\circ$.

The time difference Δt between the two fragments was measured feeding the signals from MWPC2 to the start and the one from MWPC1 to the stop input of a time-to-amplitude converter. The signals from both MWPCs contain the information on the energy deposition ΔE_1 and ΔE_2 of particles passing through the detectors.

For normalization of the beam current, a silicon surface barrier detector with the solid angle of 1.96 msr was mounted at 27.5° relative to the beam direction.

An example for the accumulated events is shown in Fig. 1. The data were obtained at a center-of-mass energies $E_{\text{c.m.}} =$ 160.0 MeV for reactions at the middle of the target. Plot (a) shows the events on the ϕ_{12} vs θ_{12} plane with the bin size of 0.5° for both $\Delta\phi_{12}$ and $\Delta\theta_{12}$. Figure 1(b) shows the plot on the $(\Delta t, \Delta E_1 + \Delta E_2)$ plane, but for events in the rectangular region in Fig. 1(a). Fission events form an arrowhead distribution are well separated from the elastically scattered projectile-target events. The appearance of these events at large Δt values means that the projectile-like nuclei enter MWPC2 and the target-like nuclei enter MWPC1. In the opposite case of target-like nuclei entering MWPC2 and projectile-like nuclei entering MWPC1, the target-like nuclei have kinetic energies of ~10-15 MeV and are not able to pass through both the gas-shielding foil and the electrode foil of the detector. In this case no ϕ_2 signal is generated.

Figure 1(c) also shows the events on the ϕ_{12} vs θ_{12} plane, but for events located within the fission gate marked in Fig. 1(b). The FMT fission events are located in the elliptic region.

In Fig. 1(c) we recognize fission events of different origin, which have a lower folding angle but a wide distribution in ϕ_{12} symmetric to 180°. These events are due to fissions of target-like nuclei after nucleon transfer. A smaller folding angle θ_{12} means that the projectile-like nucleus is scattered into backward direction after the transfer, resulting in larger recoil velocity of the fissioning nucleus.

We define the FMT fission events as those recorded within the fission gate marked in Fig. 1(b) and the FMT gate in marked in Fig. 1(c).

III. RESULTS AND DISCUSSIONS

The cross section for the FMT fissions (σ_{fiss}) are shown in Fig. 2 as a function of the center-of-mass energy $E_{\text{c.m.}}$. The values were determined from the angular distribution

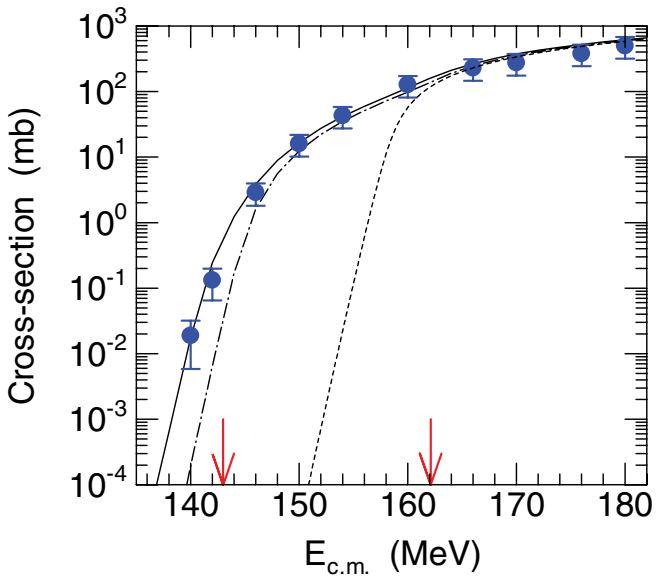

FIG. 2. (Color online) Cross sections for the full momentum transfer (FMT) fission of the reaction ^{36}S+^{238}U. Curves represent the results of coupled-channel calculations (see text). The Coulomb barriers for polar and equatorial collisions are at 143.0 and 162.1 MeV, respectively, as indicated by the arrows.

$d\sigma_{\rm fiss}/d\Omega(\theta_{\rm c.m.})$ in the range of $85^\circ \leqslant \theta_{\rm c.m.} \leqslant 125^\circ$. The cross sections are almost equal to those of the projectiles being captured inside the Coulomb barrier ($\sigma_{\rm cap}$). The data were fitted with a function described in [10], which was then integrated over the solid angle to yield the cross sections. Because of the limited angular range covered in our experiment, the $\sigma_{\rm fiss}$ values contain an error arising from the uncertainties in $d\sigma_{\rm fiss}/d\Omega(\theta_{\rm c.m.})$ at forward and backward angles. We estimated a 35 % uncertainty in $\sigma_{\rm fiss}$ in addition to the statistical uncertainty.

In order to determine the influence of nuclear properties on the capture cross sections, we performed a coupled-channels calculations using the computer code CCDEGEN [11]. We used the same parameters for the nuclear potential as in our previous work for the reactions ^{16}O+^{238}U and ^{30}Si+^{238}U [6,7]. The dashed curve in Fig. 2 is the result without considering any collective properties of target and projectile (one-dimensional barrier penetration model). The corresponding Coulomb barrier is at 158.1 MeV. This model does not reproduce the cross sections for $E_{\rm c.m.} < 160$ MeV. The dash-dotted curve represents the calculation taking into account the deformation of ^{238}U with $\beta_2 = 0.275$ and $\beta_4 = 0.05$ [6,7,12]. These results reproduce the data well down to $E_{\rm c.m.} = 146.0$ MeV, showing that the static deformation of ^{238}U is the main reason for the cross section enhancement at sub-barrier energies. Data at the two lowest energies of 142.0 and 140.0 MeV are reproduced, when couplings to vibrational states are additionally taken into account (solid curve). In this case the 2^+ state at 3.29 MeV in ^{36}S ($\beta_2 = 0.16$ [13]) and the 3^- state at 0.73 MeV in ^{238}U ($\beta_3 = 0.086$ [14]) were considered.

Figure 3 shows the mass distributions for the FMT fissions. The fragment masses were determined by using the

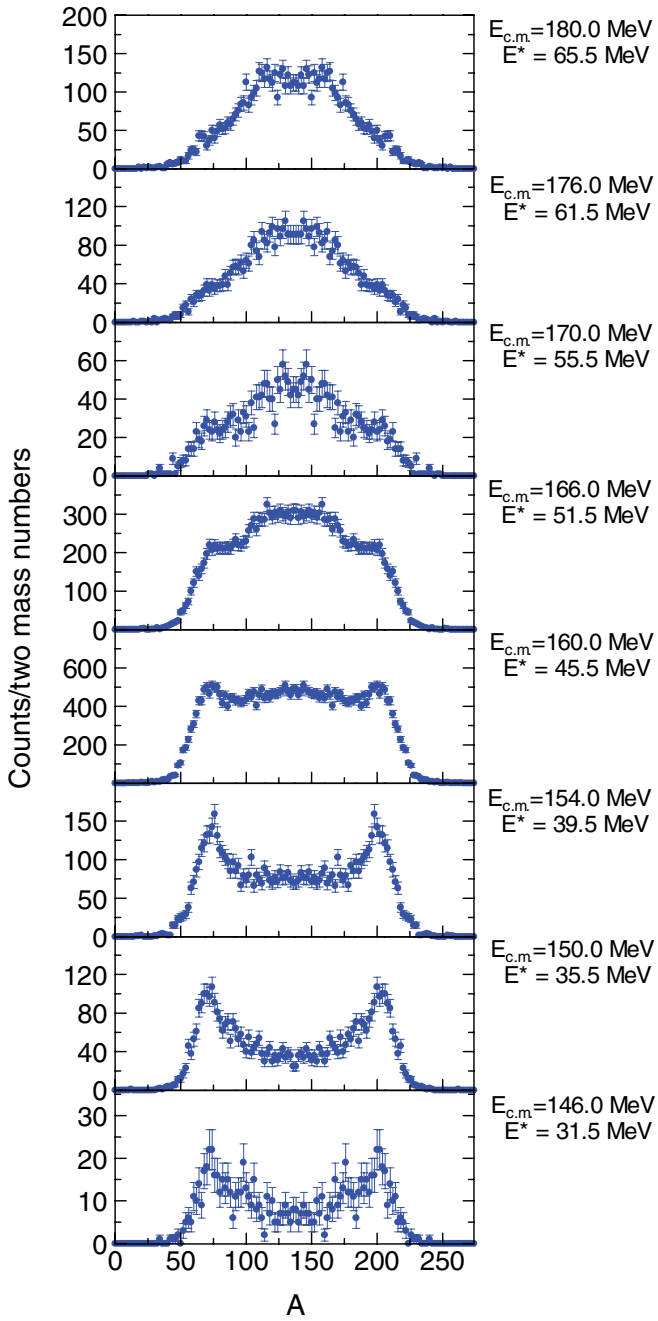

FIG. 3. (Color online) Mass distributions for FMT fissions of the reaction ^{36}S+^{238}U. Reaction energies $E_{\rm c.m.}$ and excitation energies E^* of the compound nucleus are given.

conservation law for momentum and mass with the assumption that mass of the composite system is $A_{\rm c} = 274$. The mass resolution was determined to be 8.5 (FWHM) from the peak of the elastically scattered events.

At the two highest energies of 180.0 and 176.0 MeV, the mass distributions are symmetric. With decreasing bombarding energy an additional asymmetric mass distribution becomes evident. A remarkable change occurs at sub-barrier energies of $E_{\rm c.m.} < 160.0$ MeV, where distribution becomes dominantly asymmetric with peaks at $A_{\rm H} = 200$ and $A_{\rm L} = 74$.

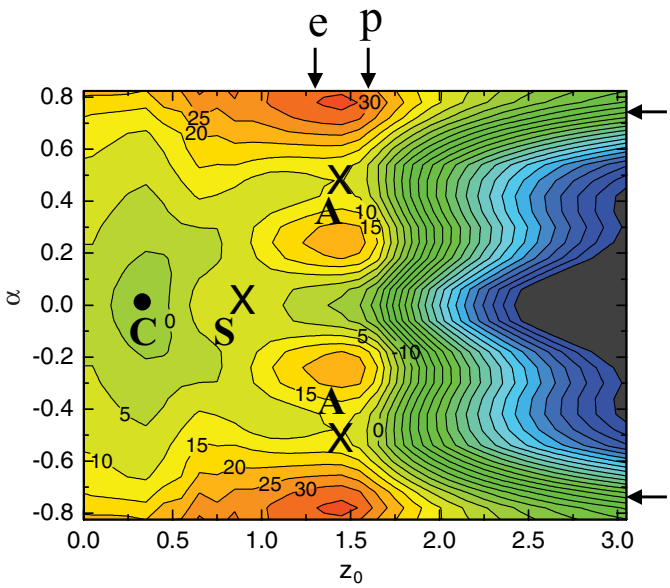

FIG. 4. (Color) Potential energy for the nucleus ^{274}Hs relative to the ground state energy of a liquid drop model. The energy is labeled in MeV and the contours are plotted with 5 MeV steps. The shape at the ground state (•) is marked by **C**. The saddle points for symmetric (**S**) and asymmetric shapes (**A**) are marked (×). The α values at the nuclear contact in collisions are indicated by the arrows on the right side, and the z_0 values for the polar (**p**) and equatorial (**e**) collisions are marked on the upper side.

In Fig. 3 we do not show the mass distributions corresponding to the lowest two energies of $E_{\text{c.m.}} = 142.0$ MeV and 140.0 MeV shown in Fig. 2 because of the low statistics.

A systematic study of reactions with ^{238}U target nuclei shows that the mass distribution changes from symmetry to asymmetry with increasing the mass of the projectile [15,16]. This phenomenon was attributed to an increased quasifission probability. The present results from the ^{36}S+^{238}U reaction reveal symmetric fission at above-barrier energies with characteristics of fusion-fission and an asymmetric one at deep sub-barrier energies with characteristics of quasifission. The contributions of the two components to the total cross section vary gradually with the beam energy.

The variation of the mass distribution with reaction energy results from the orientation effects of the deformed target nucleus ^{238}U on the reaction. At deep sub-barrier energy, where only polar collisions lead to nuclear contact, most of the reactions with projectile and target captures inside the Coulomb barrier do not form a compound nucleus, but disintegrate by quasifission into fragments around $A_{\text{H}} \approx 200$ and $A_{\text{L}} \approx 74$.

Properties for quasifission fragments were measured in reactions leading to more lighter composite systems [17]. The quasifission has asymmetric mass distribution and the angular distributions are not symmetric around $\theta_{\text{c.m.}} = 90^\circ$ but show forward-backward asymmetry. In the present experiment for ^{36}S +^{238}U, detection angles do not cover the range enough to discuss such a forward-backward asymmetry. The mass distributions shown in Fig. 3 are obtained from the angular range where the ratio of quasifission events to fusion-fission events is smaller than those for the more forward and backward angles, so that the observed enhancement of asymmetric fissions in the sub-barrier region should represent properties of the reaction ^{36}S +^{238}U.

The potential energy surface E_{pot} for the nucleus ^{274}Hs as functions of the mass asymmetry $\alpha = (A_{\text{H}} - A_{\text{L}})/(A_{\text{H}} + A_{\text{L}})$ and the center separation z_0 is plotted in Fig. 4. The E_{pot} values were calculated using the modified two-center harmonic oscillator shell model [18]. The fragment deformation δ is assumed to be zero. Two isolated fission paths are evident. The symmetric one at $\alpha = 0.0\,(A_{\text{H}} = A_{\text{L}} = 137)$ extends to the right side of the mass-symmetric saddle point marked by **S**. The asymmetric channel is at $\alpha = 0.4\,(A_{\text{H}} = 192$ and $A_{\text{L}} = 82)$ and starts at the mass-asymmetric saddle point marked by **A**.

Because the symmetric saddle point is lower and closer to the compound nucleus (marked by **C**) than the asymmetric saddle point, compound-nucleus fission proceeds preferably along the symmetric fission valley, whereas the measured asymmetric fission for the reaction ^{36}S +^{238} U at sub-barrier energy is reasonably well explained by the asymmetric fission channel. In this case the ratio of mass numbers $(A_{\text{H}}/A_{\text{L}} = 200/74)$ is equivalent to $\alpha = 0.46$. Responsible for the existence of the asymmetric fission path are the high binding energies of the fragments near the double magic nuclei ^{208}Pb and ^{78}Ni. Recent potential energy calculations based on a five dimensional deformation space obtained a similar asymmetric fission channel with $A_{\text{H}} \approx 200$ [19].

In the reaction of ^{36}S+^{238}U having mass asymmetry $\alpha = 0.74$ at the nuclear contact in collisions, the nuclear shape start to evolve from the center distance $z_0 = 1.6$ for the polar collisions (marked by **p** in Fig. 4) and $z_0 = 1.3$ for the equatorial collisions (**e**). Despite the simplification in the calculation of the potential energy surface of Fig. 4, that is the nuclear deformation δ is assumed to be zero and the nuclear shape is axially symmetric which is not the case for equatorial collisions, we can draw the following conclusions. In the case of equatorial collisions, the system has already a smaller z_0 value than the saddle point **A**. Due to the attractive nuclear forces the system develops with high probability into the direction of the compound nucleus **C**. At the polar collisions the z_0 value at the contact configuration is larger than the saddle point **A**, so that the composite system is driven into the valley of reseparation into two quasifission fragments. In addition the gradient of the potential changes the mass symmetry from $\alpha = 0.74$ to smaller values. However, due the ridge between

the asymmetric and symmetric fission valleys, the quasifission stays at $\alpha = 0.4$.

In the more asymmetric reaction ^{26}Mg+^{248}Cm, which leads to the same compound nucleus ^{274}Hs* as in ^{36}S+^{238}U, hassium evaporation residues were produced from sub-barrier to above-barrier energies [20]. Excitation energies were in the range from $E^* = 36$ to 54 MeV. The measured cross sections were reproduced by a statistical model calculation assuming that fusion occurs independently from the nuclear orientation. The fragment mass distributions for ^{26}Mg+^{248}Cm [9] show a symmetric shape in the measured energy range from $E^* = 32$ to 63 MeV, which is characteristic for a fusion-fission process. Coulomb repulsion is less strong in the reaction ^{26}Mg+^{248}Cm compared to ^{36}S+^{238}U, which results in fusion also in the case of polar collisions.

In conclusion, we have measured the mass distributions for the full momentum transfer fissions of ^{36}S+^{238}U. The distributions change from symmetry to asymmetry when energies are decreased from above-barrier to sub-barrier values. The asymmetric fission component can be attributed to quasifission, and the variation of the mass distribution with energy can be explained by the relative intensities for fusion-fission and quasifission. The results reveal the influence of the orientation of the deformed target nucleus ^{238}U on fusion.

ACKNOWLEDGMENTS

The authors thank the crew of the JAEA-tandem facility for the beam operation. Special thanks are due to Dr. Y. Aritomo of FLNR in Dubna for the calculation of the potential energies in Fig. 4. Thanks are also due to Dr. A. Iwamoto of JAEA, Dr. T. Ichikawa of RIKEN and Dr. P. Möller of LANL for fruitful discussions. This work was supported by a Grant-in-Aid for Scientific Research of the Japan Society for the Promotion of Science.

[1] S. Hofmann and G. Münzenberg, Rev. Mod. Phys. **72**, 733 (2000).
[2] K. Morita *et al*., J. Phys. Soc. Jpn. **73**, 1738 (2004).
[3] Yu. Ts. Oganessian, J. Phys. G **34**, R165 (2007).
[4] K. Nishio, H. Ikezoe, S. Mitsuoka, and J. Lu, Phys. Rev. C **62**, 014602 (2000); S. Mitsuoka, H. Ikezoe, K. Nishio, and J. Lu, *ibid.* **62**, 054603 (2000).
[5] Yu. Ts. Oganessian *et al*., Phys. Rev. C **70**, 64609 (2004).
[6] K. Nishio *et al*., Eur. Phys. J. A **29**, 281 (2006).
[7] K. Nishio *et al*., Phys. Rev. Lett. **93**, 162701 (2004).
[8] D. J. Hinde, M. Dasgupta, J. R. Leigh, J. C. Main, C. R. Morton, J. O. Newton, H. Timmers *et al*., Phys. Rev. C **53**, 1290 (1996).
[9] M. G. Itkis *et al*., Nucl. Phys. **A787**, 150c (2007).
[10] R. Vandenbosch and J. R. Huizenga, *Nuclear Fisson* (Academic Press, New York, 1973).
[11] Modified version of the CCFULL code, K. Hagino *et al*., Comput. Phys. Commun. **123**, 143 (1999).
[12] D. J. Hinde *et al*., Phys. Rev. Lett. **74**, 1295 (1995).
[13] S. Raman *et al*., At. Data Nucl. Data Tables **36**, 1 (1987).
[14] R. H. Spear *et al*., At. Data Nucl. Data Tables **42**, 55 (1989).
[15] J. Tôke *et al*., Nucl. Phys. **A440**, 327 (1985).
[16] W. Q. Shen *et al*., Phys. Rev. C **36**, 115 (1987).
[17] G. N. Knyazheva *et al*., Phys. Rev. C **75**, 064602 (2007).
[18] A. Iwamoto *et al*., Prog. Theor. Phys. **55**, 115 (1976).
[19] T. Ichikawa *et al*., Phys. Rev. C **71**, 044608 (2005, private communication).
[20] J. Dvorak *et al*., Phys. Rev. Lett. **97**, 242501 (2006); J. Dvorak *et al*., Phys. Rev. Lett. **100**, 132503 (2008).